

Received May 2, 2021, accepted May 14, 2021, date of publication May 21, 2021, date of current version June 3, 2021.

Digital Object Identifier 10.1109/ACCESS.2021.3082564

A Resolution-Enhanced Digital Micromirror Device (DMD) Projection System

YIJING ZHANG^{1,2}, PHIL SURMAN³, AND SAILING HE^{1,2,4}, (Fellow, IEEE)

¹Centre for Optical and Electromagnetic Research, National Engineering Research Center for Optical Instruments, Zhejiang University, Hangzhou 310058, China

²Ningbo Research Institute, Zhejiang University, Ningbo 315100, China

³The Photonics Institute, Nanyang Technological University, Singapore 639798

⁴Department of Electromagnetic Engineering, School of Electrical Engineering, KTH Royal Institute of Technology, 100 44 Stockholm, Sweden

Corresponding author: Sailing He (sailing@zju.edu.cn)

This work was supported in part by the National Key Research and Development Program of China under Grant 2017YFA0205700, in part by the National Natural Science Foundation of China under Grant 61774131 and Grant 11621101, in part by the Ningbo Science and Technology Project under Grant 2020G012, and in part by the Fundamental Research Funds for the Central Universities under Grant 2019FZA5002.

ABSTRACT In this paper we present a resolution-enhanced system for digital micromirror device (DMD) projected images by utilizing time multiplexing and birefringence in order to achieve this with static components only. This provides a less expensive solution than reducing the size of the hardware pixels and can also be applied to higher resolution displays, as and when, these become available. Birefringent materials have different refractive indices for linearly polarized light with orthogonal polarization directions. A high-resolution projected image can be observed by overlapping two or three native resolution images at shifts of one half or one third of a DMD pixel diagonal respectively on successive frames. The optical components comprise a custom-made quartz plate as the birefringent component and an off-the-shelf twisted nematic liquid crystal display (TN-LCD) screen as a polarization rotator that is synchronized with the DMD frame rate. This paper covers the principle of operation and the system design. The functioning of the display is verified using enlarged images of the letter ‘R’ and a checkerboard pattern that are formed from a small number of DMD pixels.

INDEX TERMS Birefringence, digital micromirror device (DMD), resolution enhancement, static components.

I. INTRODUCTION

In the display field, pixels are the units that carry information, and higher resolution means that a larger number of pixels can be displayed, which means that a larger amount and denser data display becomes possible. A convenient starting point for the assessment of the perceived resolution is that for 20/20 vision where the eye can resolve features subtending one minute of arc, which corresponds to 30 cycles per degree [1]. This was the basis for the term ‘retina display’ that was applied to iPhones. The criterion is a simplification; however, if it is met then the display will have reasonably acceptable quality. With current direct-view displays, such as TVs, monitors and phones, there is generally no problem. Virtual reality (VR) and augmented reality (AR) displays with their requirement for a large field of view can suffer from insufficient display panel resolution and may show the

‘screen-door effect’ where the pixel boundaries are visible as mentioned in [2], [3].

In VR, AR and projection displays, it is practicable to apply some form of resolution enhancement as the display panels in these devices are small. Nevertheless, an enhancement technique has been demonstrated on a monitor where the screen is physically moved in a circular path by employing a spinning weight [4]. Super-resolution in microscopy is described in [5]. In [6], a projector that uses native resolution light modulator panels to enhance projection resolution at selected regions is presented, which is achieved by decomposing a target high resolution image into a sparse edge image and a complementary lower resolution non-edge image, and then projecting these images in a time sequential manner at a high frame rate. Various techniques for sequential superimposition in projectors are given in [7].

Improvement in near eye displays is described in [8] [9] and [10]. And in [11], a display structure that cascades two-layered spatial light modulators (SLMs) is proposed

The associate editor coordinating the review of this manuscript and approving it for publication was Norbert Herencsar¹.

combined with an image decomposition algorithm, the structure achieves double spatial resolution and double refresh rate by making two panels produce fixed lateral displacements that are refreshed at staggered intervals; This is an example of multiplicative superposition, unlike the others referenced here which are additive. In [8], a compact active static component is proposed to address the accommodation–convergence conflict problem and enhance image resolution in a light field near eye display by using a birefringent plate and a twisted nematic switch cell. Pancharatnam-Berry phase components [Geometrical Phase Optical Components: Measuring Geometric Phase without Interferometry] are employed in [9], [12]. The displays of [10] and [13] incorporate holographic optical elements.

Although typical image capture devices tend to have a higher resolution than the panel on which they are displayed, there has been considerable research on enhancing the captured image [14]–[16]. References [17] presents an interesting method of enhancing the edges in areas of the image that are moving, for example, scrolling script. In some other popular imaging fields, such as metasurface imaging display as mentioned in [18] [19], [20], the enhancement of resolution can also be of great significance.

We were inspired by techniques from related research [7] to complete a digital micromirror device (DMD) projection display system that can achieve resolution multiplication, but without using any moving parts. In this system, we use a laser as the illumination source, a twisted nematic-liquid crystal display (TN-LCD) screen as the light polarization rotator device and a field programmable gate array (FPGA) circuit to drive the TN-LCD screen in synchronism with the DMD. We customized the birefringent crystal elements in accordance with the pixel size of the DMD and the wavelength of the laser, designed the optical path and completed the construction of the entire system. For image detection, we used a charge-coupled device (CCD) to obtain experimental results and MATLAB to analyze the results of the projected images.

Rather than focusing on algorithm research, we concentrated on the construction and design of the system and aimed to provide a solution for realizing the resolution enhancement in the DMD projection system. This article introduces the principle in the second chapter, the system design in the third chapter, the experiment and result analysis in the fourth chapter, the discussion in the fifth chapter, and the conclusion in the sixth chapter.

II. PRINCIPLE

The overall operating principle of the system is shown in the schematic diagram in Fig. 1. The light emitted by the laser is unpolarized and is input to the subsequent system. After passing through the polarizer, the light beam becomes linearly polarized with the same polarization direction as the polarizer; it then enters a polarization rotator vertically. The polarization rotator is used to change the polarization direction of the linearly polarized light, allowing the beam to continuously switch between two orthogonal linearly

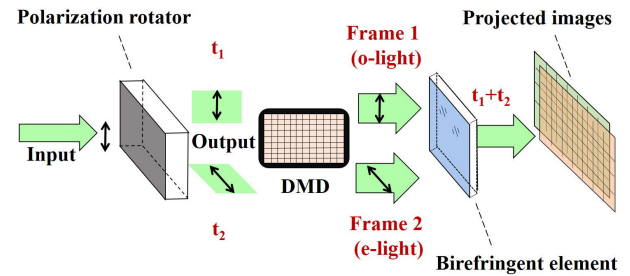


FIGURE 1. Overall operating principle schematic diagram of the proposed DMD projection system with enhanced resolution.

polarized states. The DMD is used to load frame images from the computer and provide projected images by reflection. Due to birefringence, two orthogonal linearly polarized beams are produced that correspond to ordinary light (o-light) and extraordinary light (e-light), and as a result, the projected images shift a certain distance. Based on time multiplexing, superimposed projected images can be obtained which enables a DMD projection system with multiplied resolution to be realized.

A. TIME MULTIPLEXING

Resolution-enhanced images can be obtained by shifting and superimposing multiple projected images at different times [16], [21]. As shown in Fig. 2, different frames are projected by the DMD at different times. The shift of these images is sub-pixel and in the direction of the DMD pixel diagonal. Therefore, when these projected images are superimposed, an original projection pixel will effectively be blended into several smaller projection pixels. In this way, the resolution of DMD projected images can be enhanced. As shown in Fig. 2, the letter S represents the diagonal distance of a DMD pixel. If the shift distance of projected images is $1/2 S$ and two images are superimposed, an original projection pixel can be blended into 2 small projection pixels on each side, which means that the resolution can be doubled. If the shift distance of the projected images is $1/3 S$ and three images overlap, an original projection pixel can be blended into 3 small projection pixels on each side, which means that the resolution can be tripled. The system introduced in this article achieves the effect of 2 times the native projection resolution.

The critical flicker frequency (CFF) threshold is the critical frequency at which a flickering image appears to be continuous to observers; it has different values for different people and is lower with decreasing screen luminance [22]. Since 60 Hz exceeds the CFF value of most people in the environment with the ambient illumination not exceeding one foot-candle (approximately 11 lux), and at the luminance not exceeding 10 cd/m^2 of the display [22], they will not feel obvious flicker when viewing the projected image at this frequency in the same or lower illumination environment. Then, due to the persistence of vision described in [23] and [24], the human eye merges the images displayed at

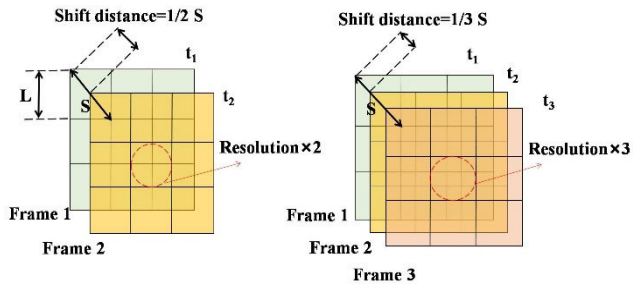


FIGURE 2. Time-multiplexed images: (a) the superimposed image with double resolution and (b) the superimposed image with triple resolution.

adjacent times and it seems that these images are displayed at the same time. By these characteristics of the human eye, time multiplexing [4], [11], [21] can be realized.

B. BIREFRINGENT COMPONENT

A quartz plate is introduced as the birefringent element as shown in Fig. 3 [8]. The ordinary and extraordinary rays have refractive indexes of n_o and n_e respectively, so the projected images of o-light and e-light will have different projected positions after passing through the quartz plate. The dispersion angle ϕ between the o-light and the e-light is given by:

$$\phi = \theta - \tan^{-1}\left(\frac{n_o^2}{n_e^2} \tan \theta\right) \quad (1)$$

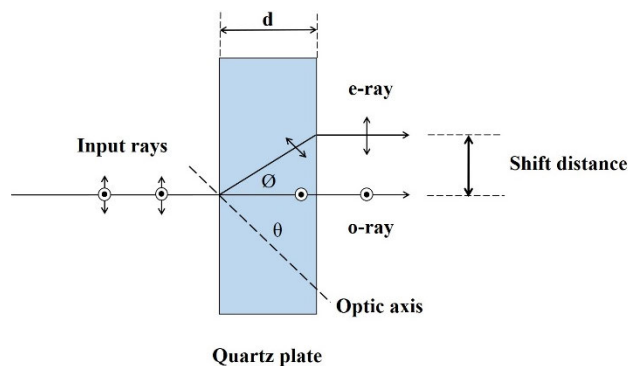


FIGURE 3. Schematic diagram for birefringence in a quartz plate.

where θ is the elevation angle between the optic axis and input rays, and it is 45° [8].

Because the polarization directions of the o-light and e-light are perpendicular to each other, a twisted nematic (TN) liquid crystal device can be used as the polarization rotator. As shown in Fig. 4, when the TN device is in state 1, the liquid crystal molecules are arranged parallel to each other, and the polarization direction of the input rays does not change. When the TN device is in state 2, the liquid crystal molecules are arranged in a twisted nematic column with two surface molecules perpendicular to each other. When the polarization direction of the input linearly polarized light is same with the direction of surface molecules, it changes with the molecular arrangement direction in the TN device. Therefore, the

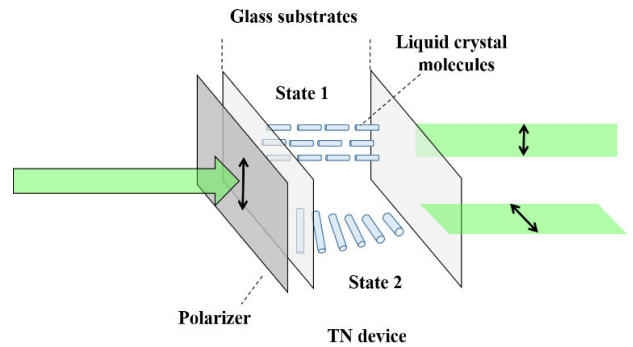


FIGURE 4. Schematic diagram for a twisted nematic liquid crystal device as a polarization rotator.

polarization direction of the output linearly polarized light changes 90° compared with the input light.

III. SYSTEM DESIGN

The experimental system comprises three parts: the optical components, the optical path design and the circuits and code program design.

A. OPTICAL COMPONENTS

1) THE BIREFRINGENT ELEMENT

The custom-made quartz plate is shown in Fig. 5; the rotation angle of optical axis from the surface of the quartz plate is consistent with that shown in Fig. 3; that is 45° . When a 532 nm wavelength laser beam passes through the plate, the refractive index n_o of o-light is 1.54689, and the refractive index n_e of e-light is 1.55609. According to Eq. (1), the dispersion angle ϕ of o-light and e-light in the quartz plate can be calculated.

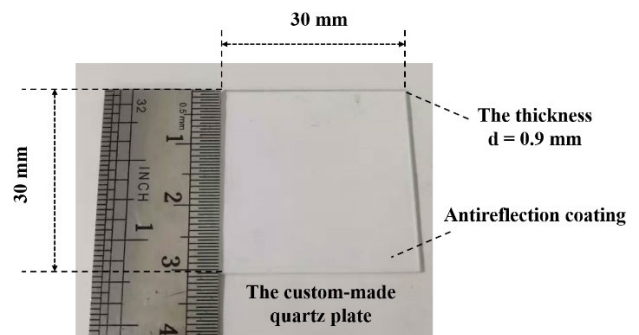


FIGURE 5. Photo of the custom-made quartz plate used in the system.

Having found ϕ , the relationship between the thickness d of the quartz plate and ϕ can be easily inferred and expressed as Eq. (2).

$$d = \frac{S/2}{\tan \phi} = \frac{\sqrt{2}L}{2 \tan \phi} \quad (2)$$

where S represents the diagonal distance of a single pixel of the DMD, and L represents the side length of a DMD pixel. If the superimposed projected image achieves two times resolution enhancement, then the shift distance of the

projected image of o-light and e-light should be $1/2 S$. The model number of the DMD in our system is DLP F6500, and the DMD pixel side length L is $7.56 \mu\text{m}$. According to Eq. (2), the thickness d of the quartz plate is 0.9 mm.

As a 532 nm laser light source is used in our system, the surface of the quartz plate is coated with an antireflection coating for this wavelength in order to improve the light transmittance.

2) THE POLARIZATION ROTATOR

The TN-LCD screen used is an ordinary computer display screen with model number A190EN02, 1280×1024 resolution, and working frequency of 60 Hz. We removed the backlight plate of the screen and the polarizer in the exit direction, that is, the rear polarizer, and only retained the front polarizer and the liquid crystal panel. The purpose is to let the laser beam pass through the polarizer and the liquid crystal panel, and then emit directly. Different states of the screen are controlled by circuits and code program, and the two states shown in Fig. 4 correspond to the black and white display of the screen respectively.

B. OPTICAL PATH DESIGN

The initial optical path structure is designed as shown in Fig. 6. The output light of the laser is a parallel beam with a diameter of about 1cm, a wavelength of 532 nm and a power of 200 mW. Since the polarization rotator of the linearly polarized light is a standard monitor screen, when it is placed behind the DMD and in front of the quartz plate, a grid projection as shown in Fig. 6 will appear, which is caused by light passing through two cascaded periodic structures: the DMD and the TN-LCD screen. The reason is the microstructure of the TN-LCD screen, as shown in Fig. 7. Each TN-LCD pixel has a part of the opaque thin film transistor (TFT) circuit control area and the black mask that accommodates the addressing lines. Only the effective area of each TN-LCD pixel can transmit light. Therefore, if a DMD projected image goes through the TN-LCD screen in the way as shown in Fig. 6, it will inevitably be covered by the pixel grid of the TN-LCD screen.

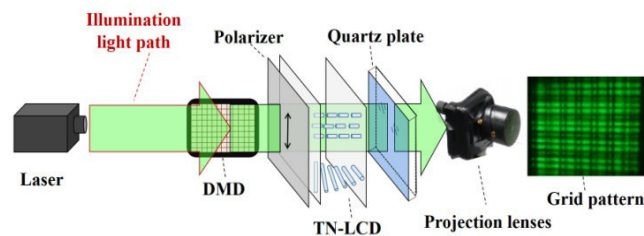


FIGURE 6. Schematic diagram of the initial optical path structure.

To solve this problem, we designed another light path structure, as shown in Fig. 7. As the laser beam itself is a wide beam with a diameter of about 1cm, a convex lens with a focal length of 35 mm is placed in front of the laser and behind the polarizer, the purpose of which is to converge the beam into a

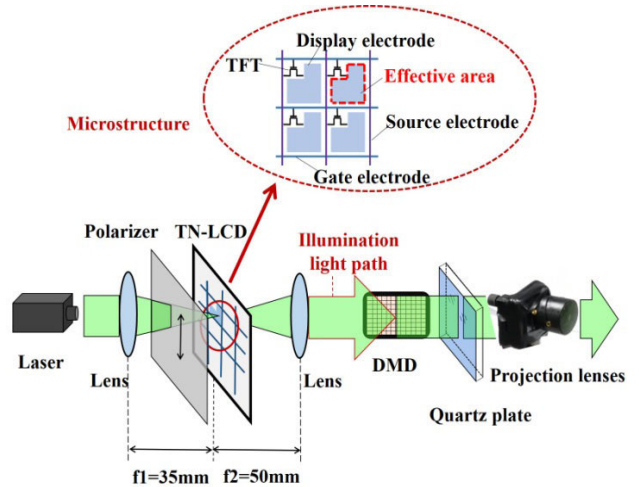


FIGURE 7. Schematic diagram of the improved optical path structure.

small region. The TN-LCD screen is located at the focal point. Under ideal conditions, adjusting the TN-LCD's position can make the focal point of laser beam exactly fall on the effective area of a single TN-LCD pixel as shown in Fig. 7. However, it is difficult to achieve in actual experiments, so we adjusted the position of the TN-LCD screen so that the focal point of laser beam falls on as few as possible of the effective areas of TN-LCD pixels. Then a convex lens with a focal length of 50 mm placed at the front of the TN-LCD screen collimates the illuminating beam again. After going through the illumination light path comprising multiple mirrors, the laser beam illuminates the DMD and forms a projected image, and then passes through the quartz plate and the projection lenses to form an enlarged projected image. Such a design not only changes the polarization direction of linearly polarized light when switching the state of the TN-LCD, but also does not form a grid pattern on the projected image.

C. CIRCUITS AND CODE PROGRAM DESIGN

The hardware circuit structure is shown in Fig. 8. The state switching of the TN-LCD screen requires two circuit boards,

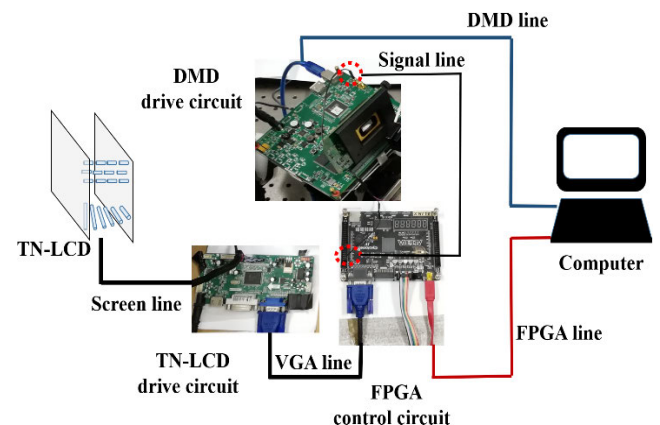


FIGURE 8. Schematic diagram for the hardware and circuit structure.

the TN-LCD driver circuit board, and the FPGA control circuit board. One end of the TN-LCD driver circuit board is connected to the TN-LCD screen with a screen line, and the other end is connected to the FPGA circuit board with a VGA line. The FPGA circuit board is also connected to a computer and can be programmed and controlled by the computer. We programmed the FPGA circuit on the computer software platform Quartus using Verilog HDL language, and then loaded the code into the FPGA circuit. In this way, the FPGA circuit can make the TN-LCD screen work between state 1 and state 2, and work at a certain frequency by controlling the TN-LCD driver circuit board.

In order to synchronize the DMD frame images with the state of TN-LCD, we slave the TN-LCD from the DMD output signal master. As Fig. 8 shows, one end of the DMD driver circuit board is connected to the computer with a DMD line, and the other end is connected to the FPGA circuit board with a signal line. Specific parameters of the DMD, such as frame images, refresh frequency and trigger signal are loaded by the computer. The DMD acts as the master by sending out a trigger signal after loading images frame 1 and frame 2. The output signal of the DMD is detected by the FPGA circuit so that the display state of the TN-LCD is controlled by the DMD.

The main structure of the code program is shown in Fig. 9. The first piece of the program for displaying DMD frame images includes two main parts: the parameter setting and image loading. The second piece of code for driving the TN-LCD includes three main modules: clock signal setting, VGA display preset and display state definition. Then the DMD and TN-LCD are prepared ready. When the DMD output signal is detected by the FPGA circuit, there is a piece of code to count the falling edge number of the signal and judge whether the count is odd or even. When the count of the DMD output trigger signal is odd, the TN-LCD screen displays in state 1, and when it is even, the TN-LCD screen displays in state 2. In this way, the synchronous change of the DMD and the TN-LCD screen can be realized.

IV. EXPERIMENT AND RESULT ANALYSIS

A. EXPERIMENT

The overall structure of the experimental system is shown in Fig. 10. When the system is running, the laser and the other devices are turned on, the DMD and TN-LCD are synchronized and the circuits loading the program are working normally. The experiment environment is dark and with an ambient illumination of 0.1 lux, and the luminance of the projected images is also further lower than the display luminance in [22]. Symbols t_1 and t_2 represent two adjacent moments at a certain frequency. At t_1 , the TN-LCD screen is in state 1, the DMD shows frame 1. The projected image is of o-light, which goes through the quartz plate and is enlarged by the projection lenses and then the projected image I_1 is detected by a CCD placed in a fixed position. In the same way, at t_2 , the TN-LCD screen is in state 2, the DMD shows frame 2. The projected light is of e-light, which goes through

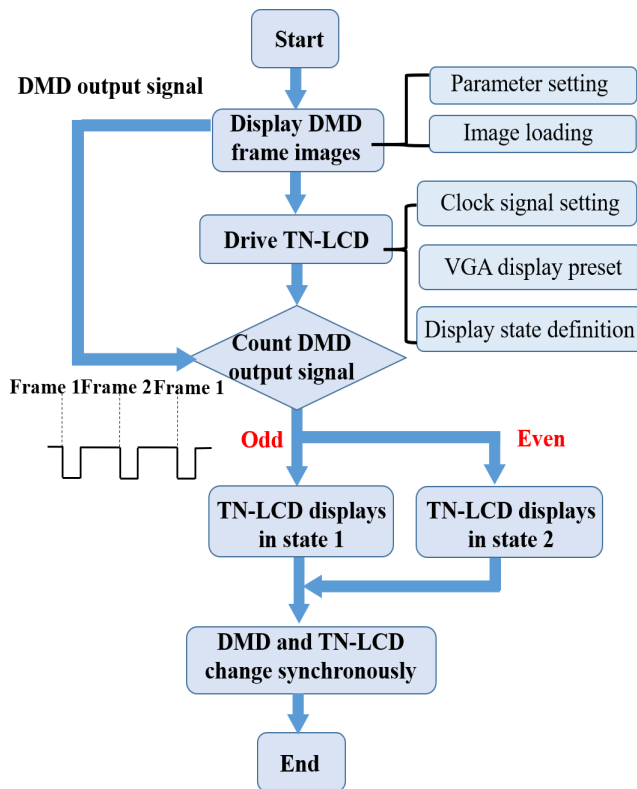


FIGURE 9. Flow chart for the main structure of our program code.

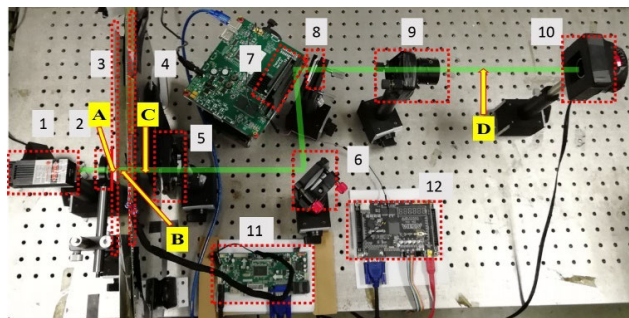


FIGURE 10. Photo of the overall structure of the experimental system: 1-laser, 2-lens, 3-polarizer, 4-TN-LCD, 5-lens, 6-mirror, 7-DMD and drive circuit, 8-quartz plate, 9-projection lenses, 10-CCD, 11-TN-LCD drive circuit, 12-FPGA circuit.

the quartz plate and is enlarged by the projection lenses and then the projected image I_2 is detected by the CCD. When the system works at a frequency of 60 Hz, the projected image is perceived as a superimposed projected image of the image I_1 and the image I_2 by the human eye.

B. RESULT ANALYSIS

In the result analysis, a CCD is used to instead of the human eye to detect projected images. In the experiment, a letter R pattern with a stepped shape and a checkerboard pattern with one pixel accuracy are used as test objects to prove the effectiveness of our system, which is formed by MATLAB software. As the letter R with the side width of 10 DMD

pixels is easy to measure the number of projection pixels and provides a lot of convenience for result analysis, it is a suitable test object for our experimental system. The projected images I_1 and I_2 detected by the CCD at t_1 and t_2 are shown in Fig. 11.

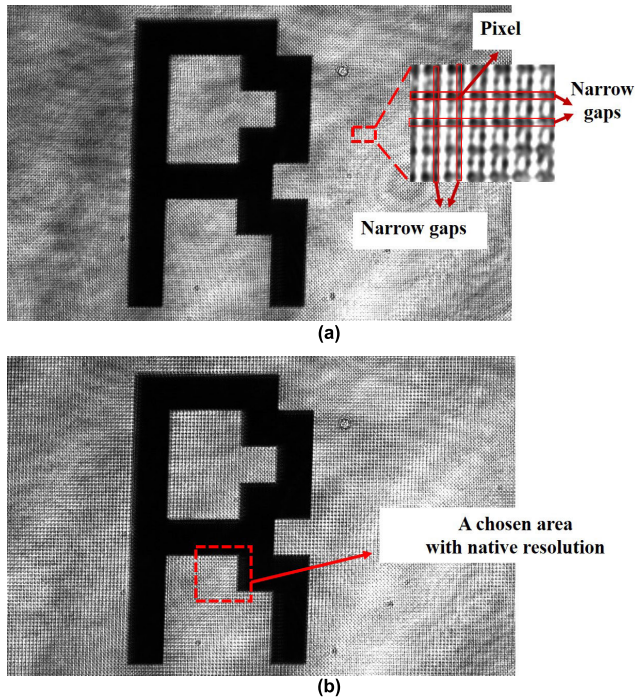


FIGURE 11. The projected images of a letter R pattern with stepped shape detected by CCD: (a) the detected image I_1 at t_1 , and (b) the detected image I_2 at the neighboring time point t_2 (the projection system works at a frequency of 60 Hz).

The schematic diagram of the magnification of projected images is shown in Fig. 12. The height of the detected projected images I_1 and I_2 , as shown in Fig. 11, is about 85 enlarged projection pixels. Then, as shown in Fig. 12, the original projected image without magnification is with a height of 85 original projection pixels, that is the same size of 85 DMD pixels. As the side length L of a DMD pixel is $7.56 \mu\text{m}$, the height h of the original projected images without magnification is $642.6 \mu\text{m}$. As the CCD is with a resolution of 1936×1216 and the CCD pixel size of $5.86 \mu\text{m}$, the height of its detected area is $7125.76 \mu\text{m}$, that is the size $m \times h$ of the enlarged projected images as shown in Fig. 12. So, it can be calculated that the magnification m of our system is about 11. At the same time, the shift distance $S/2$ is enlarged in the same proportion, and it is projected as $m \times S/2$ in the enlarged projected images.

It should be noted that the native resolution of the projected images mentioned below reflects the native resolution of the DMD device and has nothing to do with the resolution of the detector device CCD. The size of a single pixel of the enlarged projected image is $(7125.76/85) \mu\text{m}$, that is about $83.8 \mu\text{m}$. However, the side length of a single pixel of the CCD is $5.86 \mu\text{m}$, which is much smaller than the pixel

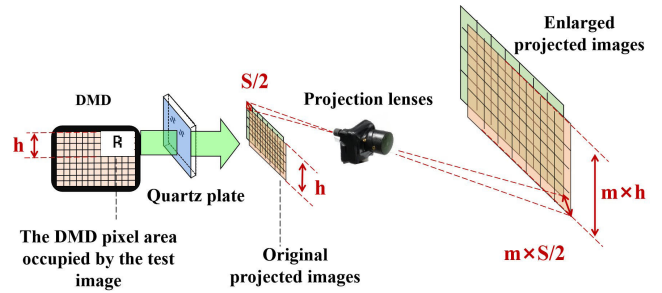


FIGURE 12. Schematic diagram of the magnification of projected images.

size $83.8 \mu\text{m}$ of an enlarged projected image after going through the projection lenses.

If the system realizes double resolution projection, the detected images I_1 and I_2 should have a certain displacement when the spatial position detected by the CCD remains unchanged. Therefore, we conducted the following image processing and analysis on the I_1 and I_2 images detected in the experiment:

To prove that the projected images at time t_1 and t_2 are shifted, we subtracted image I_1 from image I_2 in MATLAB. And the resulting image I_3 presenting the absolute difference between I_1 and I_2 is shown in Fig. 13. Because the gray scale of the letter R pattern is only black and white, the gray value of the digital image can be represented by 0 and 1, with 0 presenting black and 1 presenting white. In our MATLAB program, subtracting image I_1 from image I_2 gets only absolute values and not negative values. Therefore, if the projection pixels' gray values of image I_1 and image I_2 are the same at a certain spatial position, the projection pixel gray value of the image I_3 should be 0, which means black. If the projection pixels' gray values of image I_1 and image I_2 are different at a certain spatial position, the projection pixel gray value of the image I_3 should be 1, which means white.

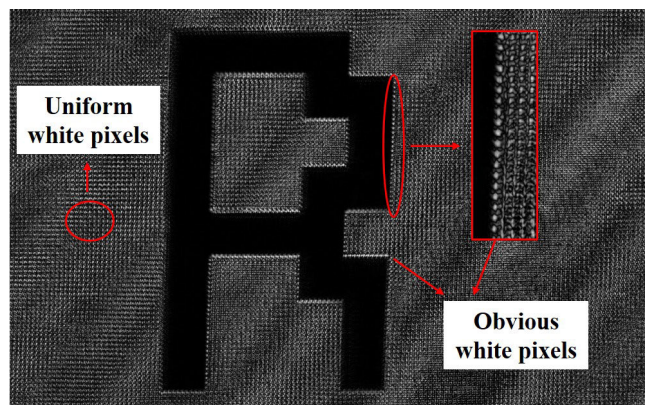


FIGURE 13. The resulting image I_3 of absolute difference values obtained by subtracting image I_1 from image I_2 with MATLAB software.

During the whole experiment, the CCD is in the same detection position. If the projected image does not shift, the image I_3 should be black. However, as shown in Fig. 13,

there are obvious white image pixels on the border of the letter R, indicating that the projected letter R has been shifted. In addition, since there are also narrow gaps among DMD pixels, as shown in Fig. 11 (a), when the projected image shifts, the image I_3 will also show a uniform distribution of smaller white image pixels compared with the white image pixels on the border of the letter R.

In order to prove that the resolution of the observed projected image is doubled, we conducted the following analysis. Since the perceived image is a superimposed image at 60 Hz under a low illumination condition [22], we simulated the superimposed projection of image I_1 and image I_2 with MATLAB, as shown in Fig. 14. We added image I_1 and image I_2 based on their display time ratio, and got the resulting image I_4 , as shown in Fig. 14. Although the image I_4 is obtained with MATLAB, it comes from two real resulting images I_1 and I_2 detected by the CCD, and it shows true information of images I_1 and I_2 . Then, the image I_4 is an effective auxiliary image to demonstrate our system and can be used to simulate the perceived image observed by human eyes directly.

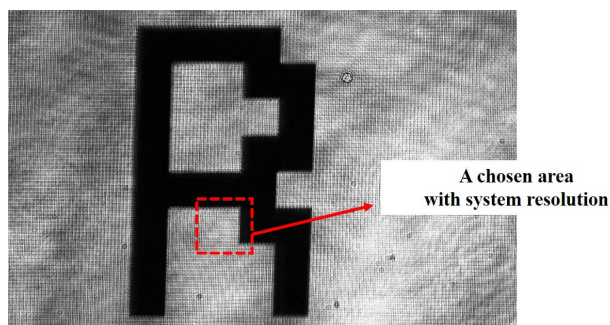


FIGURE 14. The resulting image I_4 obtained with the MATLAB software after the addition program of images I_1 and I_2 , simulating the superimposed image observed by human eyes.

Compared to image I_2 with the native resolution, image I_4 shows the resolution achieved by our system. In Fig. 15, (a) and (b) are enlarged images of the same part from image I_2 and image I_4 from Fig. 11 (b) and Fig. 14. It shows that the side width of the projected pattern letter R of the native resolution is 10 projection pixels, but when the system works at 60 Hz, the side width observed is 20 projection pixels. In Fig. 15 (c), the right part of the diagram shows the shape of real DMD pixels. It should be noted that, there is a hole in the middle of a DMD pixel which is caused by the DMD device itself. So, as the left part of Fig. 15 (c) shows, a projected pixel of image I_2 with native resolution also shows a hole in the middle and is different from the small projected pixels of image I_4 with system resolution shown in Fig. 15 (d). In Fig. 15 (d), as all original projected pixels of the chosen area are white, when projected images shift as the diagram shows, an original projected pixel will be divided into four new smaller projected pixels, as the number 1, 2, 3, and 4 marked. And all these smaller pixels are with uniform brightness. Therefore, it can prove that the

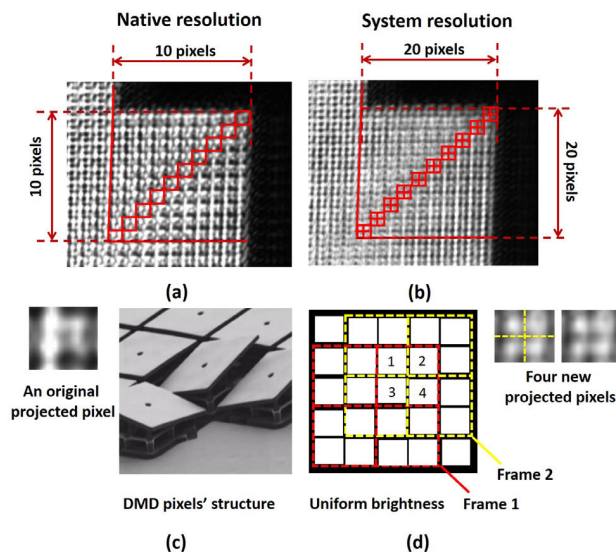


FIGURE 15. The contrast diagram of native resolution and system resolution: (a) the chosen area of image I_2 with native resolution, (b) the same chosen area of image I_4 with native resolution, (c) an original projected pixel and the structure of real DMD pixels, and (d) the schematic diagram of the formation of finer pixels realized by the system.

projection pixels realized by the experimental system are more refined than the native resolution, and the projection of twice the resolution is realized.

In order to prove that our system can also achieve resolution enhancement of fine images, following the same way, we tested a checkerboard image with one-pixel accuracy. The projected images I_{11} and I_{22} detected by the CCD at two adjacent time points t_1 and t_2 are shown in Fig. 16. The border of this tested image is designed for the convenience of experiment operation, the checkerboard area is shown in Fig. 16 (a). A checkerboard with an accuracy of one DMD pixel that means one DMD pixel is either an all-white cell or an all-black cell. The resulting image I_{44} simulating the effect of human observation is also obtained with the MATLAB software by adding images I_{11} and I_{22} and is shown in Fig. 17. The same part of image I_{22} with the native resolution and image I_{44} with the system resolution are chosen to form a contrast. The contrast diagram is shown as Fig. 18.

As show in Fig. 18, (a) and (b) are enlarged images of the same part from image I_{22} and image I_{44} from Fig. 16 (b) and Fig. 17. It can be observed that the image with system resolution has stepped edges which proves that the projected image has been shifted by the corresponding angle and distance. A column or a line corresponding to one original projected pixel is the width of two projected pixels with system resolution, as shown in Fig. 18 (b). An original projected pixel reflecting the appearance of the DMD pixel is shown in Fig. 18 (c). In Fig. 18 (d), when the projected images shift as the diagram shows, an original projected pixel will also be divided into four smaller pixels, as the numbers 1, 2, 3, and 4 marked. However, since the original white pixels of the checkerboard are distributed diagonally, and other

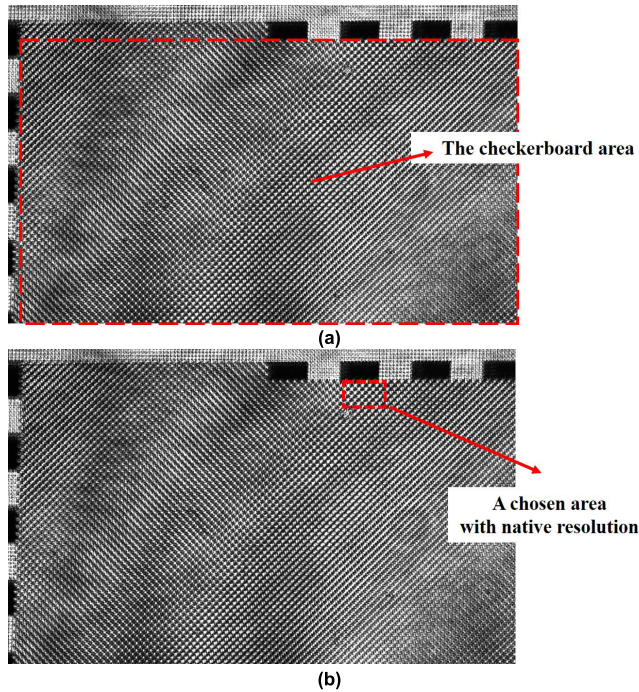


FIGURE 16. The projected images of a checkerboard pattern with the one-pixel accuracy detected by CCD: (a) the detected image I_{11} at t_1 , and (b) the detected image I_{22} at the neighboring time point t_2 (the projection system works at a frequency of 60 Hz).

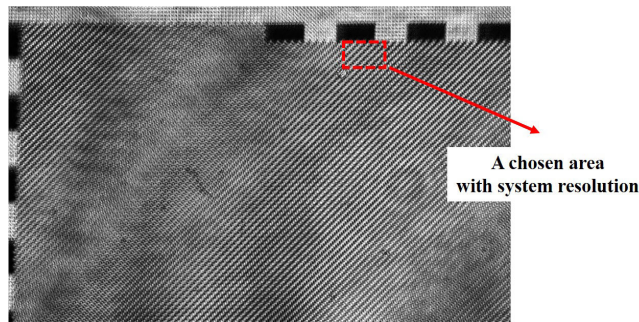


FIGURE 17. The resulting image I_{44} obtained with the MATLAB software after the addition program of images I_{11} and I_{22} , simulating the superimposed image observed by human eyes.

horizontally adjacent original pixels are black, these four new projected pixels have uneven brightness. Only the position of numbers 2 and 3 are brightest because they are overlapped by two original white projected pixels. Therefore, it can be proved that our system can also achieve double resolution enhancement of fine images.

Since this system has been proven to have twice the resolution enhancement effect, we tested another letter ‘R’ with a different shape to observe its effect in a text projection application. The projected images I_1' and I_2' detected by the CCD at two adjacent moments t_1 and t_2 are shown in Fig. 19. When the system is applied in text projection, arcs and diagonal lines always have a greater impact on the viewer’s viewing experience compared with sharp edges of straight lines, and may even cause difficulties in text distinguishment. As shown

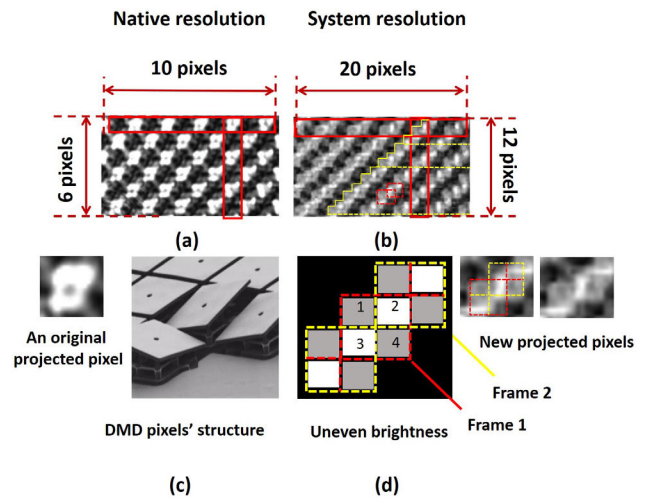


FIGURE 18. The contrast diagram of native resolution and system resolution: (a) the chosen area of image I_{22} with native resolution, (b) the same chosen area of image I_{44} with native resolution, (c) an original projected pixel and the structure of real DMD pixels, and (d) the schematic diagram of the formation of finer pixels realized by the system.

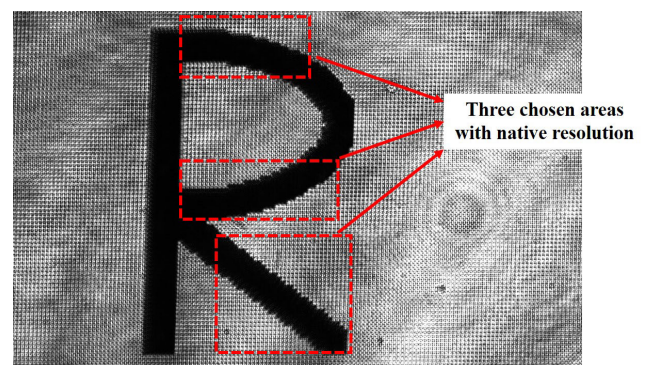
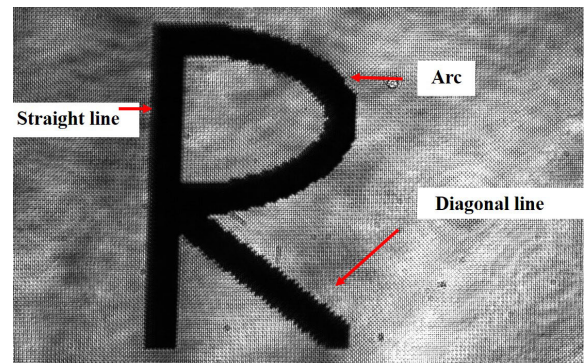


FIGURE 19. The projected images detected by CCD in a text projection application: (a) the detected image I_1' at t_1 , and (b) the detected image I_2' at the neighboring time point t_2 (the projection system works at a frequency of 60 Hz).

in Fig. 19 (a), because the letter R with this shape is composed of the three main shapes of characters; straight line, diagonal line, and arc, it is an appropriate choice of application to test the effect of our system.

In the same way as before, we added image I_1' and image I_2' based on their display time ratio with MATLAB, and got the resulting image I_4' , as shown in Fig. 20. Then, image I_4' simulates the superimposed image by human observation. Comparing image I_2' shown in Fig. 19 (b) and image I_4' shown in Fig. 20, it can be observed that the letter R of image I_4' becomes smoother than that of image I_1' or image I_2' .

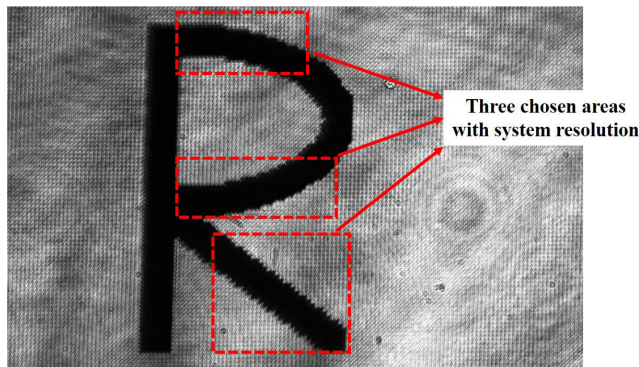


FIGURE 20. The resulting image I_4' obtained with the MATLAB software after the addition program of images I_1' and I_2' , simulating the superimposed image observed by human eyes.

For the convenience of observation, we have enlarged the same areas of image I_2' and image I_4' to form contrast images, as shown in Fig. 21. In Fig. 21, the upper parts of the images are the chosen areas from image I_2' , and the lower parts of the images are the same chosen areas from image I_4' . It can be observed that in our projection system, the sharp edges with native resolution can be shown as soft, that is, smoother. Therefore, in addition to having the effect of increasing the number of projection pixels, our system is useful for improving the image quality and text readability to some extent.

V. DISCUSSION

A. DISADVANTAGES

1) LOW TRANSMISSION EFFICIENCY

Although the standard output power of the laser in our system is 200 mW, the actual optical power entering the system as an illumination beam is far lower than that. This is because 2-lens shown in Fig. 10 only partially collects the light emitted from the laser, and the rest of the light is lost. Therefore, as shown in Fig. 10, the point between 2-lens and 3-polarizer is set as point A, and the optical power P_A measured at point A is regarded as the actual input optical power P_{in} of our system. Similarly, the point between 9-projection lenses and 10-CCD is set as point D, and the optical power P_D measured at point D is regarded as the output optical power P_{out} of our system. Then, the transmission efficiency E of this system can be calculated by Eq. (3).

$$E = (P_{out} / P_{in}) \times 100\% \quad (3)$$

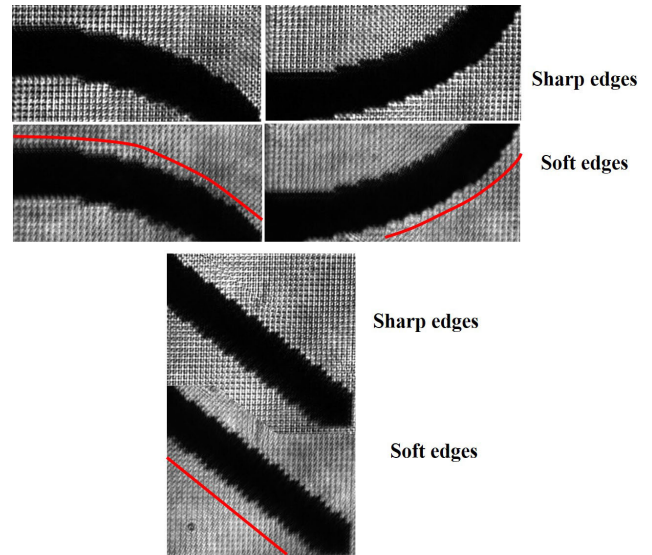


FIGURE 21. Enlarged contrast images for the same parts of image I_2' and image I_4' .

In addition, we also measured the optical power P_B and P_C at point B between 3-polarizer and 4-TN-LCD and point C between 4-TN-LCD and 5-lens to observe the optical transmission process of the system and analyze the influence of each device on the transmission efficiency. Table 1 shows the mean of 5 sets of optical power data measured under stable system operation and the calculated overall mean transmission efficiency E of our system.

From Table 1, the average value of transmission efficiency E is calculated to be 3.93%, which is relatively low. We analyzed the reasons for the energy loss between each point. As shown in Fig. 10, the light loss between point A and point B is caused by 3-polarizer, because 3-polarizer only allows light that is consistent with its polarization direction to pass through, and the rest of the light is absorbed or reflected. The light loss between point B and point C is caused by the 4-TN-LCD: In addition to reflection, the TN-LCD also absorbs part of the light energy and converts it into heat, and the pixel grid structure of the TN-LCD itself also blocks part of the light from passing through.

TABLE 1. Optical power and transmission efficiency.

	P_A (mW)	P_B (mW)	P_C (mW)	P_D (mW)	E
1	110.0	58.76	29.15	4.030	3.67%
2	101.5	62.60	31.08	4.098	4.04%
3	110.5	61.55	32.85	4.450	4.03%
4	103.5	60.32	31.98	4.060	3.92%
5	98.80	57.80	28.43	3.958	4.01%
MEAN	104.9	60.20	30.70	4.119	3.93%

There are several reasons for the light loss between point C and point D: First, the light reflected by the mirror is not completely used by the area where the DMD loads the

image, and a considerable part of the light is reflected to other directions without participating in imaging process; Second, the light participating in imaging is reflected by the DMD to form some multi-order diffraction projected images, and the unwanted diffraction orders cause significant loss [25]; Third, transmissive devices, such as 5-lens, the 8-quartz plate and the 9-projection lenses, suffer a degree of absorption and surface reflection losses; Finally, reflective devices, such as the mirror 6 and the DMD, have reflection losses.

2) SLIGHT BLURRED IMAGES

In our experimental results, the images detected by CCD as shown in Fig. 11, Fig. 16 and Fig. 19 are slight blurred on the edges, which is principally caused by DMD diffraction imaging and aberration [26]. Since each pixel of the DMD is equivalent to a micro-mirror, and these micro-mirrors constitute the periodic structure of the DMD, then the DMD is equivalent to a periodically distributed grating. In the experiment, when the illumination beam with a wavelength of 532nm is reflected by the DMD, multiple diffraction orders are formed. Diffraction not only causes the loss of optical energy as discussed above, but also causes undesired diffraction orders to enter the projection lenses and introduces aberrations, so edges of the test images are slight blurred.

To solve this problem in subsequent research, adding a spatial filter to block undesired diffraction orders, or correcting aberrations as a separate research subject may be effective methods [25], [26]. Some methods with metasurfaces may also be effective in eliminating high-order images, enlarging field of view, and improving image contrast [19], [20].

B. ADVANTAGES

Compared with other solutions that have been proposed by researchers, the principal difference of our system is the introduction of the TN-LCD device. Although the polarization rotator can be realized by some kinds of other devices with no multiple-pixel structure as described in [7]–[9], and [12], our solution has many advantages for achieving super-resolution and has great value in application and research. Since a TN-LCD has many pixels that can be independently controlled, this makes it more advantageous than some other devices in the following aspects:

1) MORE RELIABLE

TN liquid crystal devices are prone to lose twisted nematic order and lose their effect. If it happens due to some reasons in the experiment or product applications, such as excessive light intensity [27], individual LC devices with a single working area used in other solution [8] need to be replaced with new ones, but a TN-LCD does not. Because only a few pixels of the TN-LCD are used, even if they are damaged, the TN-LCD itself will not be greatly affected due to the independence of each TN-LCD pixel. We can replace the damaged TN-LCD pixels with the other available but not need to replace a new TN-LCD.

2) MORE SCALABLE

Since all pixels of the TN-LCD can be controlled independently, a TN-LCD can be divided into multiple independent working areas by programming the control program code, which makes the same effect of integrating countless individual LC devices on one TN-LCD. This allows a TN-LCD to modulate multiple illuminating beams at the same time in some cases, such as the application shown in Fig. 22, unlike other individual rotators with no multiple-pixel structure that require the same number of illuminating beams under the same circumstances. Therefore, our system avoids excessive increase in the number of more polarization rotators and provides convenience for subsequent experiments and further research.

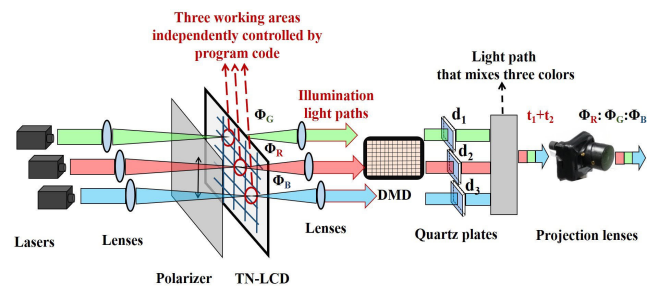


FIGURE 22. Schematic diagram of a possible structure applied to color projection display that is based on our system.

3) MORE NOVEL

Due to some obvious disadvantages caused by TN-LCD grid structure and others, no one has modulated the illuminating light in such a projection light path using a TN-LCD. It is a novel and interesting solution using a normal screen to achieve resolution enhancement in projection system and provides a new idea for wide beam modulation and even multi-beam modulation.

4) MORE EFFICIENT

Since it takes a longer period and higher cost to make an optical element with the same effect of a TN-LCD, choosing the available TN-LCD is an efficient solution to achieve the same experimental results. For setting the entire system, it saves both time and cost. It is also an effective solution that could be implemented quickly and performed reliably to test the effectiveness of a system prototype and is easy to get updated by further research.

C. OTHER APPLICATIONS

1) MONOCHROME PROJECTION WITH OTHER COLORS

This system can be applied to monochromatic light projection of other wavelengths. When the wavelength of illuminating beam changes, the refractive index n_o and n_e of the quartz plate are different from that in our system [28], [29]. Then, the thickness d of the quartz plate varies with the refractive index n_o and n_e from Eq. (1) and Eq. (2). Therefore, when our

system is applied to a monochromatic light projection system of different wavelengths, the quartz plate of the corresponding thickness d needs to replace the original, and the same resolution-enhanced effect can be realized.

2) COLOR PROJECTION

When the system is applied to color projection, three main illuminating lights of red, green, and blue are required at the same time [18], [20]. We proposed a possible solution for a color projection based on our system, and the schematic diagram is shown in Fig. 22. As mentioned before, a TN-LCD can be divided into three independent working areas by changing the program code. So, arrangement states of liquid crystal molecules of the three areas of the TN-LCD can be changed to different degrees, in other words, the ratio $\Phi_R : \Phi_G : \Phi_B$ of the luminous flux of the three colors after passing through the TN-LCD can be controlled. As mentioned before, quartz has a dispersion effect on light of different wavelengths [28], [29], so three quartz plates of different thicknesses d_1 , d_2 , and d_3 should be used. Then, a color projection with resolution enhancement may be realized by mixing three individual projected images of three colors.

In theory, our system has the feasibility of color projection applications, but further research is needed on some issues. To solve the problem that three beams of light incident on a DMD at the same time, perhaps different incident directions will be a feasible solution. The small birefringence difference of quartz material may cause an over-thick quartz plate and may reduce the transmission efficiency. Some other components using a medium with a larger birefringence in relation to its dispersion, such as liquid crystal [33] may overcome this problem.

VI. CONCLUSION

This experimental system was proposed to provide a specific solution that can achieve resolution multiplication of DMD projected images with static components only. In our proof of principle system, a readily available TN-LCD screen is used as the polarization direction rotator, a custom-made quartz plate is used to utilize birefringence, an improved optical path is designed to accommodate the microstructure of the TN-LCD screen, and the circuits and code program design makes the devices work normally and synchronously. According to observation and the analysis of the CCD detected results, the system realizes the DMD projection display with double resolution and has the effect of making edges smoother in the text projection application. Then, the disadvantages and advantages of this system, and possible implementations for other applications are discussed.

For subsequent research, improvements can be proposed from the following three aspects. Firstly, the system may be combined with related image algorithms to improve the quality of the projected images. Secondly, faster rotators such as pi cells [30], [31], [32] or other types [33] [34] can be used to improve the viewing experience. Thirdly, based on this experimental system, multiple cascaded polarization

rotators may be used to achieve triple or multiple resolution enhancement. Currently we are working on increasing the luminance and raising the perceived frame rate to higher frequency.

Obtaining higher resolution in projection display devices is becoming increasingly difficult due to decreasing the hardware pixel size. Full high definition (HD) [35] can currently be converted to the equivalent of 4K ultra high definition (UHD) [36] with the use of actuators [4], [7] that must have physical movement. Looking to the future, we have shown that it may be possible to convert a 4K device to the equivalent of 8K operation but without the use of any moving parts and therefore providing a less expensive solution.

REFERENCES

- [1] G. Westheimer, "Optical superresolution and visual hyperacuity," *Prog. Retinal Eye Res.*, vol. 31, no. 5, pp. 467–480, Sep. 2012, doi: [10.1016/j.preteyeres.2012.05.001](https://doi.org/10.1016/j.preteyeres.2012.05.001).
- [2] W. S. Cho, J. Y. Park, C. S. Choi, S.-H. Cho, S. Baek, and J.-L. Lee, "Air-gap-embedded robust hazy films to reduce the screen-door effect in virtual reality displays," *Nanoscale*, vol. 12, no. 16, pp. 8750–8757, Apr. 2020, doi: [10.1039/c9nr10615d](https://doi.org/10.1039/c9nr10615d).
- [3] G. Tan, Y. Lee, T. Zhan, J. Yang, S. Liu, D. Zhao, and S. Wu, "Foveated imaging for near-eye displays," *Opt. Exp.*, vol. 26, no. 19, pp. 25076–25085, Sep. 2018, doi: [10.1364/OE.26.025076](https://doi.org/10.1364/OE.26.025076).
- [4] F. Berthouzoz and R. Fattal, "Resolution enhancement by vibrating displays," *ACM Trans. Graph.*, vol. 31, no. 2, pp. 1–14, Apr. 2012, doi: [10.1145/2159516.2159521](https://doi.org/10.1145/2159516.2159521).
- [5] K. Zhanghao, J. Gao, D. Jin, X. Zhang, and P. Xi, "Super-resolution fluorescence polarization microscopy," *J. Innov. Opt. Health Sci.*, vol. 11, no. 1, Jan. 2018, Art. no. 1730002, doi: [10.1142/S1793545817300026](https://doi.org/10.1142/S1793545817300026).
- [6] B. Sajadi, M. Gopi, and A. Majumder, "Edge-guided resolution enhancement in projectors via optical pixel sharing," *ACM Trans. Graph.*, vol. 31, no. 4, pp. 1–12, Jul. 2012, doi: [10.1145/2185520.2185575](https://doi.org/10.1145/2185520.2185575).
- [7] R. Byanju, S. A. J. Hansen, and M. N. Akram, "A comparative study of superimposition techniques for enhancing the projector resolution: Simulations and experiments," *Displays*, vol. 55, pp. 80–89, Dec. 2018, doi: [10.1016/j.displa.2018.11.002](https://doi.org/10.1016/j.displa.2018.11.002).
- [8] J.-Y. Wu, P.-Y. Chou, K.-E. Peng, Y.-P. Huang, H.-H. Lo, C.-C. Chang, and F.-M. Chuang, "Resolution enhanced light field near eye display using e-shifting method with birefringent plate," *J. Soc. Inf. Display*, vol. 26, no. 5, pp. 269–279, May 2018, doi: [10.1002/jsid.665](https://doi.org/10.1002/jsid.665).
- [9] Y. Lee, T. Zhan, and S. Wu, "Enhancing the resolution of a near-eye display with a Pancharatnam-Berry phase deflector," *Opt. Lett.*, vol. 42, no. 22, pp. 4732–4735, Nov. 2017, doi: [10.1364/OL.42.004732](https://doi.org/10.1364/OL.42.004732).
- [10] J. S. Lee, Y. K. Kim, M. Y. Lee, and Y. H. Won, "Enhanced see-through near-eye display using time-division multiplexing of a Maxwellian-view and holographic display," *Opt. Exp.*, vol. 27, no. 2, pp. 689–701, 2019, doi: [10.1364/OE.27.000689](https://doi.org/10.1364/OE.27.000689).
- [11] F. Heide, D. Lanman, D. Reddy, J. Kautz, K. Pulli, and D. Luebke, "Cascaded displays: Spatiotemporal superresolution using offset pixel layers," *ACM Trans. Graph.*, vol. 33, no. 4, pp. 1–11, Jul. 2014, doi: [10.1145/2601097.2601120](https://doi.org/10.1145/2601097.2601120).
- [12] S. Moon, S.-W. Nam, Y. Jeong, C.-K. Lee, H.-S. Lee, and B. Lee, "Compact augmented reality combiner using Pancharatnam-Berry phase lens," *IEEE Photon. Technol. Lett.*, vol. 32, no. 5, pp. 235–238, Mar. 1, 2020, doi: [10.1109/LPT.2020.2968340](https://doi.org/10.1109/LPT.2020.2968340).
- [13] S. Lee, C. Jang, S. Moon, J. Cho, and B. Lee, "Additive light field displays," *ACM Trans. Graph.*, vol. 35, no. 4, pp. 1–13, Jul. 2016, doi: [10.1145/2897824.2925971](https://doi.org/10.1145/2897824.2925971).
- [14] J. Xu, Y. Liang, J. Liu, and Z. Huang, "Multi-frame super-resolution of Gaofen-4 remote sensing images," *Sensors*, vol. 17, no. 9, pp. 2142–2157, Sep. 2017, doi: [10.3390/s17092142](https://doi.org/10.3390/s17092142).
- [15] X. Zhang, C. Li, Q. Meng, S. Liu, Y. Zhang, and J. Wang, "Infrared image super resolution by combining compressive sensing and deep learning," *Sensors*, vol. 18, no. 8, pp. 2587–2602, Aug. 2018, doi: [10.3390/s18082587](https://doi.org/10.3390/s18082587).

- [16] H. Zhu, X. Tang, J. Xie, W. Song, F. Mo, and X. Gao, "Spatio-temporal super-resolution reconstruction of remote-sensing images based on adaptive multi-scale detail enhancement," *Sensors*, vol. 18, no. 2, pp. 498–518, Feb. 2018, doi: [10.3390/s18020498](https://doi.org/10.3390/s18020498).
- [17] P. Didyk, E. Eisemann, T. Ritschel, K. Myszkowski, and H.-P. Seidel, "Apparent display resolution enhancement for moving images," *ACM Trans. Graph.*, vol. 29, no. 4, pp. 1–8, Jul. 2010, doi: [10.1145/1778765.1778850](https://doi.org/10.1145/1778765.1778850).
- [18] X. Li, L. Chen, Y. Li, X. Zhang, M. Pu, Z. Zhao, X. Ma, and M. H. X. L. Y. Wang, "Multicolor 3D meta-holography by broadband plasmonic modulation," *Sci. Adv.*, vol. 2, no. 11, pp. 1–6, 2016, doi: [10.1126/sciadv.1601102](https://doi.org/10.1126/sciadv.1601102).
- [19] J. Guo, T. Wang, B. Quan, H. Zhao, C. Gu, J. Li, X. Wang, G. Situ, and Y. Zhang, "Polarization multiplexing for double images display," *Opto-Electron. Adv.*, vol. 2, no. 7, pp. 1–6, 2019, doi: [10.29026/oea.2019.180029](https://doi.org/10.29026/oea.2019.180029).
- [20] F. Zhang, M. Pu, P. Gao, J. Jin, X. Li, Y. Guo, X. Ma, J. Luo, and A. X. L. H. Yu, "Simultaneous full-color printing and holography enabled by centimeter-scale plasmonic metasurfaces," *Adv. Sci.*, vol. 7, pp. 1–10, 2020, doi: [10.1002/advs.201903156](https://doi.org/10.1002/advs.201903156).
- [21] B. Lee, D. Yoo, J. Jeong, S. Lee, D. Lee, and B. Lee, "Wide-angle speckle-less DMD holographic display using structured illumination with temporal multiplexing," *Opt. Lett.*, vol. 45, no. 8, pp. 2148–2151, Apr. 2020, doi: [10.1364/ol.390552](https://doi.org/10.1364/ol.390552).
- [22] B. R. Hammond and B. R. Wooten, "CFF thresholds: Relation to macular pigment optical density," *Ophthalmic Physiol. Opt.*, vol. 25, no. 4, pp. 315–319, Jul. 2005.
- [23] H. L. Hawkins and G. L. Shulman, "Two definitions of persistence in visual perception," *Perception Psychophys.*, vol. 25, no. 4, pp. 348–350, Jul. 1979, doi: [10.3758/BF03198815](https://doi.org/10.3758/BF03198815).
- [24] R. Rennie, "Making images that move," *Teach. Sci.*, vol. 61, no. 3, pp. 6–9, Sep. 2015.
- [25] I. Alsolami and W. Heidrich, "Imaging with SPADs and DMDs: Seeing through diffraction-photons," *IEEE Trans. Image Process.*, vol. 29, pp. 1440–1449, 2020, doi: [10.1109/TIP.2019.2941315](https://doi.org/10.1109/TIP.2019.2941315).
- [26] Y. Wang, H. Li, Q. Hu, R. Chen, X. Lv, and S. Zeng, "Extending the 3D scanning range of DMD-based scanners for femtosecond lasers," *Opt. Lett.*, vol. 45, no. 24, pp. 6639–6642, Dec. 2020, doi: [10.1364/OL.409862](https://doi.org/10.1364/OL.409862).
- [27] X. Liu, L. Peng, Y. Gao, Y. Zhao, Y. Liu, D. Li, M. Zhu, Z. Cao, J. Shao, and X. Wang, "Laser damage characteristics of indium-tin-oxide film and polyimide film," *Infr. Phys. Technol.*, vol. 99, pp. 80–85, Jun. 2019, doi: [10.1016/j.infrared.2019.03.028](https://doi.org/10.1016/j.infrared.2019.03.028).
- [28] B. C. Zelinschi, C. Dascălu, R. Stănculescu, and D. O. Dorohoi, "Simulation of the main refractive indices of quartz crystal from maramures area," *Ann. Univ. Dunarea De Jos Galati Fascicle II Math. Phys. Theor. Mech.*, vol. 34, no. 1, pp. 54–58, 2011.
- [29] M. J. Abuleil and I. Abdulhalim, "Birefringence measurement using rotating analyzer approach and quadrature cross points," *Appl. Opt.*, vol. 53, no. 10, pp. 2097–2104, Apr. 2014.
- [30] M. Xu, D. K. Yang, P. J. Bos, X. Jin, F. W. Harris, and S. Z. D. Cheng, "11.4L: Late-news paper: Very high pretilt alignment and its application in Pi-cell LCDs," in *SID Symp. Dig. Tech. Papers*, vol. 29, no. 1, 2012, pp. 139–142, doi: [10.1889/1.1833713](https://doi.org/10.1889/1.1833713).
- [31] P. J. Bos and K. R. Koehler/Beran, "The pi-cell: A fast liquid-crystal optical-switching device," *Mol. Crystals Liquid Crystals*, vol. 113, no. 1, pp. 329–339, Dec. 1984, doi: [10.1080/00268948408071693](https://doi.org/10.1080/00268948408071693).
- [32] G. V. Simonenko, S. A. Studentsov, and V. A. Ezhov, "Choosing the optimum design for an optical shutter based on a π -cell," *J. Opt. Technol.*, vol. 80, no. 9, pp. 537–541, Jan. 2013, doi: [10.1364/JOT.80.000537](https://doi.org/10.1364/JOT.80.000537).
- [33] H. Wang, O. Yaroshchuk, X. Zhang, Z. Zhuang, P. Surman, X. W. Sun, and Y. Zheng, "Large-aperture transparent beam steering screen based on LCMPA," *Appl. Opt. Opt. Technol. Biomed. Opt.*, vol. 55, no. 28, pp. 7824–7829, Oct. 2016, doi: [10.1364/AO.55.007824](https://doi.org/10.1364/AO.55.007824).
- [34] P. F. Mcmanamon, P. J. Bos, M. J. Escuti, J. Heikenfeld, S. Serati, H. Xie, and E. A. Watson, "A review of phased array steering for narrow-band electrooptical systems," *Proc. IEEE*, vol. 97, no. 6, pp. 1078–1096, Jun. 2009, doi: [10.1109/JPROC.2009.2017218](https://doi.org/10.1109/JPROC.2009.2017218).
- [35] R. Kay, "High-definition TV," *Computerworld*, vol. 42, no. 42, pp. 34–35, 2008.
- [36] J. Yurek, "Ultra high definition: Beyond pixel count," *IEEE Consum. Electron. Mag.*, vol. 4, no. 4, pp. 89–91, Oct. 2015, doi: [10.1109/MCE.2015.2463296](https://doi.org/10.1109/MCE.2015.2463296).



YIJING ZHANG received the B.E. degree in optoelectronic information science and engineering from Sichuan University, Chengdu, China, in 2018. She is currently pursuing the M.S. degree with the Centre for Optical and Electromagnetic Research, Zhejiang University, Hangzhou, China. Her current research interests include projector design, display technology, and holographic application.



PHIL SURMAN received the Ph.D. degree in head tracking two-image 3D television displays from De Montfort University, U.K., in 2003. He worked on four EU-funded 3D projects and wrote the proposals for two of them, such as MUTED and HELIUM 3D. In 2013, he was invited to write a proposal for a 3D display project by Nanyang Technological University, Singapore. The proposal was successful and resulted in the five year, 9M SGD Towards the Reality of 3D Imaging and Display Project. He worked as a Senior Research Fellow for the duration of that project. He is currently working on glasses-free vision correction for mobile devices.



SAILING HE (Fellow, IEEE) received the Licentiate of Technology and Ph.D. degrees in electromagnetic theory from the Royal Institute of Technology (KTH), Stockholm, Sweden, in 1991 and 1992, respectively. Since then, he has been worked as an Associate Professor and a Full Professor with the Royal Institute of Technology. He is also a Distinguished Professor with Zhejiang University and the Director of the joint Research Center (JORCEP) with KTH and ZJU. He has first-authored one monograph and authored/coauthored about 700 articles in refereed international journals. His current research interests include subwavelength photonics and sensing applications. He is a Fellow of the Optical Society of America (OSA), the International Society for Optical Engineering (SPIE), and the Electromagnetics Academy.

...